Optimization of multi-arm robot locomotion to reduce satellite disturbances during in-orbit assembly

Jean-Pascal Lutze
German Aerospace Center (DLR)
Institute of Robotics and Mechatronics
Münchner Str. 20, 82234 Weßling, Germany
Jean-Pascal.Lutze@dlr.de

Robert Schuller, Hrishik Mishra,
Ismael Rodríguez, Máximo A. Roa
German Aerospace Center (DLR)
Institute of Robotics and Mechatronics
Münchner Str. 20, 82234 Weßling, Germany
{Robert.Schuller, Hrishik.Mishra,
Ismael.RodriguezBrena, Maximo.Roa}@dlr.de

***Abstract*—Traditionally, manufacturing and assembly of space assets is performed on ground before sending them into orbit. However, this monolithic approach involves high launch costs due to increasing asset sizes, e.g., large telescopes for space observation. Alternatively, in-orbit assembly of space structures after launching the raw materials to orbit opens wider possibilities at a reduced cost. Mobile robotics, such as walking manipulators or multi-arm robots, are a critical component for this approach due to their mobility in orbit. However, unlike terrestrial assembly tasks, the continuous motion of the robot and materials, coupled with the change of inertial properties of the structure, results in a rotational deviation of the platform due to conservation of angular momentum in orbit. This might violate the tolerance limits of the platform antenna's cone angle for communication with the ground stations. Although exploiting the attitude control system of the platform is a straightforward solution, it might lead to issues related to the associated actuators like reaction wheels saturation, high-frequency vibration, or high fuel consumption.**

To deal with this problem, in this paper we formulate the attitude disturbance problem as a minimization of the effects created by the gait of the walking manipulator. Investigating the dynamic coupling between the robot system and the space structure gives a deeper understanding of the spacecraft's behavior depending on the robot gaits. The paper proposes a controller that optimizes the forces that the robotic arm applies to the structure, hence minimizing the base rotation. As an application, we use a space structure composed of identical elements, namely the mirrors of a segmented telescope, endowed with standard interfaces to allow the robot locomotion. We show the effects of optimizing these interaction forces in various scenarios and positions on the structure through multiple dynamic simulations.

TABLE OF CONTENTS

1. INTRODUCTION

Mankind has been historically driven by the need for exploration and discovery. Nowadays, our next frontier (and hope) is space exploration. However, ambitious goals for space exploitation are limited by the rockets' limited payload volume capacity, which restricts the size of structures used in space. As an alternative, in-space assembly technologies are currently under active investigation. These technologies not only allow to build bigger structures in orbit, but also diminish the cost of assembly and maintenance of such systems. To achieve such goal, autonomous robotic systems is a technology that needs to be maturated to the point of being applicable in these assembly tasks.

One of the main research questions for In-Space-Assembly (ISA) is how to deliver parts from the storage to the desired place on the structure. Solutions like rail systems or free-floating robots have been proposed, both with certain limitations. Rail systems require first the construction of the mobility system before the assembly can be performed, and free-floating systems offer higher flexibility but at the cost of much higher fuel consumption [1]. An alternative method is the use of robots that can walk over the structure as it is being built. This solution has two main advantages: First, it relies only on electrical energy, which can be produced with solar arrays, and second, the robot locomotes using grasping points on the structure, which provide higher confidence on the robustness of the attachment and locomotion actions of the robot. However, a robot that walks on top of a free floating structure will inevitably perturb its orientation due to the conservation of momemtum. This can lead to a misalignment of the satellite, resulting in a communication interruption with the ground station. These disturbances could be corrected by the attitude control system, up to the limit of possible saturation of the reaction wheels, or at the cost of wasteful consumption of fuel. In this work, we propose a solution to minimize the base disturbance of the satellite while the robot walks over the structure. As a result, the satellite reduces the use of the reaction wheels and thrusters. As a case study, we use in this paper the Multi-Arm Robot (MAR) developed within the ESA study MIRROR [2], see Figure 2. This project analyzes the construction of the primary mirror for a telescope, made out of several identical hexagonal mirror tiles. The MAR used for this purpose is composed of a torso and two arms. This robot can grasp the mirror tiles and place them in desired positions, and also walk over the already-built structure. Both robot arms and the single tiles have Standard Interconnects (SI) as end effectors.

In order to minimize the disturbances created by the motion of a walking robot on the spacecraft, we formulate an

978-1-6654-9032-0/23/$31.00 ©2023 IEEE

 DOI: 10.1109/AERO55745.2023.10115776

optimization problem that minimizes the forces and torques exerted by the end effectors on the satellite. Note that unlike walking robots on Earth, where feet can only create forces (push) against the ground, we can produce wrenches in the six Degrees of Freedom (DoF) via the SIs, allowing the robot to push or pull against the satellite if required. Additionally, the gravity effects on the robot structure can be ignored. Since the MAR is highly redundant, the optimization problem is too complex to be solved in a general way. To reduce this complexity, we introduce several approximations of the system. First, we propose a simplified description of the locomotion on the floating platform by combining the inertias of the robot and the assembly. This allows to represent the forces applied by the MAR to the satellite as a continuously moving grasping point to which the robot is connected via a virtual leg. This virtual leg produces forces and torques in its grasping point. These forces and torques enable the robot to follow a given trajectory, and at the same time, they are responsible for the satellite attitude perturbations. With this formulation, we propose an instantaneous QP optimization to compute the forces and torques that enable the robot to move from one point to the other while minimizing the base perturbation. We verify the results of this controller through dynamics simulations of the system that verify the effects on the base rotation, and also show the performance when perturbations are applied to the system.

This work is structured as follows. Section 2 includes a review of related work. Section 3 provides a description of the proposed dynamics formulation. The optimization formulation is provided in Section 4. The numerical experiments to verify the approach are given in Section 5, followed by the conclusions and future work in Section 6.

2. RELATED WORK

This section provides an overview of related work on the topics of in space assembly, locomotion systems in space applications, and optimization strategies to minimize attitude disturbances.

Autonomous Assembly In Space

Several assembly and repairing tasks have been performed in-space, mainly involving astronaut workforce, such as the repairing missions for the Hubble space telescope, or the construction of the International Space Station. However, this approach is not only expensive, but also involves high risk for the astronauts themselves. Future assembly and repairing tasks will certainly be performed by autonomous robots.

One of the first experiments to use autonomous robots in space was the ROTEX mission [3]. ROTEX was part of the Space shuttle mission D2 and showed a first implementation of teleoperation and autonomy in space. Later, the ETS-VII [4] mission tested rendezvous and docking using a chaser satellite endowed with a robot arm, and a small target satellite.

For current in-space assembly plans, the strategies consider in general that individual sub-parts are launched and later set together directly in space. A conceptual example is the SpiderFab [5], where a multi-arm robot is combined with a 3D printer. The robot can create 3D printed truss structures, walk over them and build directly in space all the required elements.

In order to develop and test different autonomous assembly strategies, the European Space Agency (ESA) has funded several studies in this direction. The project PULSAR (Prototype for an Ultra Large Structure Assembly Robot) [6] verified the autonomous assembly of a mirror composed by segmented mirror tiles, similar to the James Webb Space Telescope (JWST) [7]. The main focus of PULSAR was testing the technological viability of using a robot manipulator with SIs as end effectors for manipulating and assembling multiple parts. The project MOSAR (Modular Spacecraft Assembly and Reconfiguration) [8] developed a 7-DoF robot arm that walks over a structure made of cubic modules, representing modular components of a satellite. This project showed the feasibility of the walking manipulation technology for construction and repairing tasks using modular components.

Our work in particular is related to the ESA funded project MIRROR (Multi-arm Installation Robot for Readying ORUs and Reflectors),whose main goal is the development of a multi-arm robot for assembly tasks. The demonstration case is the assembly of a primary mirror using hexagonal mirror tiles with SIs as attachment points. The SIs used in this project are HOTDOCKs [9], see Fig.1, which allow mechanical, electrical, thermal and data connectivity for the required parts.

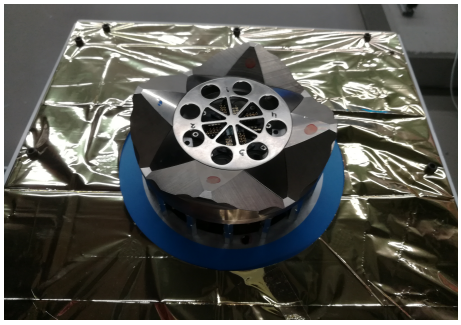

Figure 1: HOTDOCK used as an SI for an in orbital replacement unit, to support mechanical stability and energy transfers.

Locomotion Systems in Space

Reparation and assembly tasks in space imply moving and manipulating parts from their storage into designed positions. This requires in general high locomotion capabilities. For astronauts, systems such as the Manned Maneuvering Unit (MMU) [10] provide a jetpack-like vehicle that allows the astronaut to fly freely in space. These concepts are still under evolution, for instance with the NASA study FlexCraft [11].

An alternative to free floating solutions is the exploitation of the structure itself to provide locomotion support for robots. With this approach, only electrical power, instead of fuel, is needed for performing the locomotion. Moreover, the robot uses attachment points on the structure, which prevent the robot -and parts- to fly away, as they would be in general connected to the structure using a SI. This behavior was already tested and validated in space, for instance with the Canadarm2 [12] or the European Robotic Arm (ERA) [13], which can move over the International Space Station (ISS). Several projects currently work on the development of the next generation of space walking robots, including the walking manipulator developed in MOSAR [14], and the MAR system developed in MIRROR [15].

Satellite Disturbance Optimization

When a robot walks over a structure in space, perturbations on the attitude control are inevitably created. These perturbations can be negligible when the mass of the structure is much larger than the mass of the robot, as the manipulators walking on the ISS, but the disturbances can have a significant impact when the supporting structure is not as massive. These undesired rotational disturbances need to be minimized, usually by using an optimization approach.

Several approaches are available to generate and optimize an offline trajectory so that the satellite's attitude is perturbed as little as possible. In [16], a stochastic approach using STOMP [17] was employed for planning complete locomotion or assembly sequences while minimizing base perturbations. In contrast to such offline planners, Model Predictive Control (MPC) [18] approaches compute online control strategies by using a suitable cost function. Typically, state trajectories are evaluated based on the system's model over a certain time horizon, and the trajectory minimizing the cost function is selected. The first element of the resulting optimal control sequence is commanded to the system. The robot joint values can also be optimized at each time step, for instance using a Quadratic Programming (QP) formulation [19]. Here, the tasks involved in the cost function are modeled in a quadratic formulation. The QP can prioritize the different tasks, although the tasks can be violated during the resulting motion. This approach is commonly used for walking robots to stabilize the center of mass (CoM) of the robot while following a given trajectory [20]. The main drawback is that an initial trajectory is required for the optimization. Some other approaches use learning techniques to adapt the CoM trajectory online, in order to induce less contact torques at the supporting points [21].

3. Proposed Model of Locomotion on Floating Platform

This section describes the dynamics of the multi-arm robot performing locomotion on a floating platform. From the full dynamic description, we create a simplified model for control purposes, to quantify platform perturbation during locomotion.

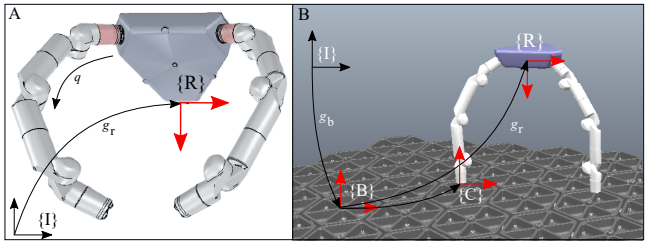

Figure 2: Modeling locomotion: A) Reference frames on the multi-arm robot; B) MAR on a floating platform.

Multi-arm Robot—The configuration of the MAR alone, see Fig. 2-A, is given by $(g_r, q) \in \mathrm{SE}(3) \times \mathbb{R}^n$, where g_r is the pose of a robot-specific frame $\{R\}$ (e.g. an end-effector) relative to the inertial frame $\{I\}$, and q includes the positions of the n revolute joints [22]. The differential kinematics of the robot frame is written as, $\dot{g}_r = g_r V_r^\wedge$, $V_r \in \mathbb{R}^6$ is the body velocity of the robot frame. The motion of the robot is described by floating-base dynamics [23, §9.4], which is written as,

$$\Lambda(q)\dot{V} + \Gamma(q, V)V = \mathcal{F} \tag{1}$$

where $V = \begin{bmatrix} V_r^\top & \dot{q}^\top \end{bmatrix}^\top$ is the total robot velocity, while $\mathcal{F} = \begin{bmatrix} \mathcal{F}_r^\top & \tau^\top \end{bmatrix}^\top$ is the total actuation consisting of the external wrench $\mathcal{F}_r \in \mathbb{R}^6$ and the joint actuation $\tau \in \mathbb{R}^n$. Furthermore, $\Lambda, \Gamma \in \mathbb{R}^{(6+n)\times(6+n)}$ are the matrices of inertia and Coriolis/centrifugal terms, respectively.

Lemma 1: Given the MAR with configuration dynamics in (1), its total generalized momentum is

$$h_r = \mathrm{Ad}_{g_r}^{-\top}(M_r V_r + M_{rq}\dot{q}) \tag{2}$$

where M_r, M_{rq} are the block matrices in the first row of Λ of (1). The energy of the multi-arm robot is written as,

$$E = \frac{1}{2} h_r^\top \underbrace{(\mathrm{Ad}_{g_r}^{-\top} M_r \mathrm{Ad}_{g_r}^{-1})^{-1}}_{\bar{M}_r} h_r + \frac{1}{2}\dot{q}^\top \Lambda_q \dot{q} \tag{3}$$

Using (2), the motion can be described alternatively as variations (dynamics) of $h_r \in \mathbb{R}^6$ and joint motion, written as

$$\frac{d}{dt} h_r(q, V) = f \tag{4}$$

$$\Lambda_q(q)\ddot{q} + \Gamma_q(q, V)V = \tau_f \tag{5}$$

where $\Lambda_q \in \mathbb{R}^{(n)\times(n)}$ and $\Gamma_q \in \mathbb{R}^{(n)\times(6+n)}$ are the reduced joint-space matrices of inertial and Coriolis/centrifugal terms, respectively. Also, $f \in \mathbb{R}^6$ is the total external wrench and $\tau_f \in \mathbb{R}^n$ is the reduced joint actuation.

Remark 1: Note that the dynamics in Lemma 1 are decoupled in inertia, which allows decoupled analysis of momentum and joint dynamics. The dynamic computations in (4) and (5) are obtained using dynamic congruent transformations of typical serial kinematic chain computations, as shown in [24].

Multi-arm Robot on Platform—Considering the locomotion of the MAR over a floating platform, see Fig. 2-B, the total configuration of the system extends the configuration of the MAR as $(g_b, g_r, \dot{q})$, where $g_b \in \mathrm{SE}(3)$ is the pose of the platform[2] relative to the inertial frame $\{I\}$, with differential kinematics $\dot{g}_b = g_b V_b^\wedge$, where $V_b \in \mathbb{R}^6$ is the platform's body velocity and $\{\bullet\}^\wedge$is the isomorphism. The equation of motion for the MAR and platform together is defined as,

$$M(q, g_r)\dot{V}_q + C(q, g_r, V_q)V_q = \mathcal{F}_q \tag{6}$$

where M and $C \in \mathbb{R}^{(6+6+n)\times(6+6+n)}$ refer to the matrices of joint-space inertia and the Coriolis/Centrifugal terms, respectively, $V_q = \begin{bmatrix} V_b^\top & V_r^\top & \dot{q}^\top \end{bmatrix}^\top$, $\mathcal{F}_q = \begin{bmatrix} \mathcal{F}_b^\top & \mathcal{F}_r^\top & \tau^\top \end{bmatrix}^\top$, $\mathcal{F}_b, \mathcal{F}_r \in \mathbb{R}^6$ are the wrenches acting on the platform and the robot frame, respectively, and $\tau \in \mathbb{R}^n$ are the joint torques.

Assumption 1: During locomotion of the MAR on the platform, *both* these systems are not externally actuated, e.g. the effects of gravity gradient, solar radiation pressure, magnetic effects or using thrusters, are not taken into account.

[2]For the MAR on the platform, g_r refers to the relative pose between the robot frame $\{R\}$ and the platform frame $\{B\}$.

Ass. 1 reflects practical operating conditions in orbit. The direct consequence of the aforementioned assumption is $\mathcal{F}_b = \mathcal{F}_r = 0_6$. Another key outcome is the conservation of the total spatial momentum, i.e.,

$$h(V_b, V) = \mathrm{Ad}_{g_b}^{-\top}\left(M_b V_b + M_{br} V_r + M_{bq}\dot{q}\right) = \text{const.} \quad (7)$$

where M_b, $M_{br} = \mathrm{Ad}_{g_r}^{-\top} M_r$, $M_{bq} = \mathrm{Ad}_{g_r}^{-\top} M_{rq}$ are the block matrices in the first row of M. As a result, the variation in the platform pose is purely due to the disturbance arising from the motion of the multi-arm robot and the conservation of h.

Furthermore, an additional holonomic constraint is imposed due to the attachment(s) between the robot and the platform, $\{C\}$ frame in Fig. 2-B, and is specified as,

$$g_c^i(g_r, q) = \text{const.} \Rightarrow V_c^i = J_c^i \dot{q} = 0_6 \quad (8)$$

where $g_c^{(\bullet)}$ refers to the pose between the platform frame $\{B\}$ and the attachment point(s) of the robot with the SI on the platform, $\{C\}$, and the superscript i refers to the index of the attachment point(s).

Hence, the complete dynamics of the locomotion of the MAR on the platform is determined by (6), under the constraints (7) and (8).

Remark 2: The constraint in (7) can be re-written with new arguments as

$$\begin{aligned} h(V_b, V) =& \mathrm{Ad}_{g_b}^{-\top}\left(M_b V_b + \mathrm{Ad}_{g_r}^{-\top}\left(M_r V_r + M_{rq}\dot{q}\right)\right) \\ =& \mathrm{Ad}_{g_b}^{-\top}\left(M_b V_b + h_r(V_r, \dot{q})\right) \end{aligned} \quad (9)$$

where h_r denotes the generalized momentum of the MAR alone, see (2) in Lemma 1, however, relative to the platform frame $\{B\}$.

A consequence of Remark 2 is that the perturbation to the platform can be analyzed as a function of the MAR's own momentum, h_r. In fact, exploiting Lemma 1, the total energy of the system is written by extending (3) as

$$E_{\text{tot}} = \frac{1}{2}\begin{bmatrix} V_b^\top & h_r^\top \end{bmatrix}\begin{bmatrix} M_b & I \\ 0 & M_r^{-1} \end{bmatrix}\begin{bmatrix} V_b \\ h_r \end{bmatrix} + \frac{1}{2}\dot{q}^\top \Lambda_q \dot{q} \quad (10)$$

Approximation of Locomotion Dynamics

A simplified model is proposed here to describe the locomotion of a MAR on a floating platform. In (10), the inertia coupling between V_b and h_r in the first term on the right hand side captures the platform perturbation due to h_r. In a typical locomotion problem, the joint dynamics serve primarily to generate the contact wrenches at $\{C\}$, which causes the desired change in h_r. We state the following assumption to simplify the model.

Assumption 2: Given a MAR that performs locomotion on a floating platform, there exists a controller to stabilize the joint dynamics ($\ddot{q}$), such that the required contact wrenches at $\{C\}$ are generated.

According to Ass. 2, the motion stabilization problem for the dynamics in (6) reduces to stabilizing the dynamics of (V_b, h_r) using the contact wrenches at the attachment point $\{C\}$. Therefore, in this paper, we model the MAR as a rigid body system, denoted by the robot frame $\{R\}$, which is able to the perform locomotion on the platform using attachment point(s) $\{C\}$, see Fig. 3. Firstly, this simplified model enables us to quantify locomotion as the variation of the robot momentum h_r, as commonly done in walking robots [24], [19]. Secondly, it also provides an intuitive way to quantify the perturbation to the platform through the momentum conservation principle, as in Remark 2. In this manner, the following work serves as a simplification of the total dynamics, and provides a first approach to deal with this novel locomotion problem. In this paper, our key contribution is determining the control law for the contact wrenches, which can be realized on a multibody robot using standard control methods to fulfil Ass. 2, see [25], [19]. In a sequel to this work, we will focus on aspects of multibody computation and control.

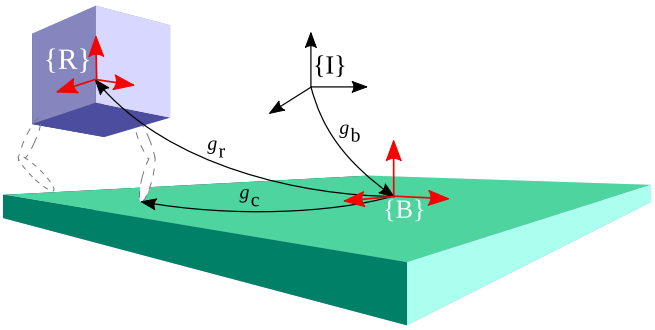

Figure 3: A simplified model of the locomotion dynamics for a multi-arm robot (approximated as a rigid body, purple cube) on a floating platform (green).

Thus, the approximated dynamics are written as the dynamics of (V_b, h_r), as

$$\begin{bmatrix} M_b & I \\ I & I \end{bmatrix}\begin{bmatrix} \dot{V}_b \\ \dot{h}_r \end{bmatrix} + \mathcal{C}(g_r, V_b, h_r)\begin{bmatrix} V_b \\ h_r \end{bmatrix} = \begin{bmatrix} -F_r \\ F_r \end{bmatrix} \quad (11)$$

where $F_r \in \mathbb{R}^6$ contains the wrenches acting on the robot frame, and $\mathcal{M}, \mathcal{C} \in \mathbb{R}^{12\times 12}$ are the matrices of inertia and Coriolis/centrifugal terms, respectively. Note that in (11), F_r creates a counter wrench on the platform due to the holonomic constraint in (8).

Assumption 3: Given the simplified model of the MAR on a platform, as shown in Fig. 3, the position of the contact point $\{C\}$ on the platform varies continuously. Which can be seen as steps with minimal increments.

Ass. 3 enables us to study the platform perturbation purely through momentum exchange with the simplified robot, without considering the hybrid dynamics of steps. This assumption can be enforced by considering infinitesimally small steps. Hence, the control problem for locomotion is to determine a control law for F_r that generates the desired motion of the rigid body (Cube) on the platform in Fig. 3. Note that F_r is not independently actuated, but it is effected through the contact wrench at $\{C\}$.

4. Control and Optimization

The objective of the proposed control approach is to track a desired trajectory for the robot relative to the base, without disturbing the attitude of the platform. The idea is to compute

a desired wrench acting on the robot frame based on the desired motion. Since the robot is underactuated due to the lack of external actuation (Assumption 1), the desired robot wrench needs to be generated by the robot's end effectors in contact with the platform. This control approach is inspired by a passivity-based whole-body controller for humanoid balancing and locomotion [20], [19], which uses a control structure similar to a PD+ controller [26].

First, a desired robot frame wrench is defined as

$$F_r^d = F_r^{ff} + F_r^{fb}, \tag{12}$$

where F_r^{ff} represents the feedforward and F_r^{fb} the feedback term. The feedforward part in (12) improves the tracking performance and is given by:

$$F_r^{ff} = \dot{h}_r^d + \mathcal{C}(g_r, V_b, h_r) \begin{bmatrix} V_b^d \\ h_r^d \end{bmatrix}. \tag{13}$$

Desired quantities of the predefined trajectory, which are provided by a high level planner, are indicated by $(\bullet)^d$. During locomotion of the MAR, the platform is supposed to hold its position. Therefore, the desired trajectory of the base is $V_b^d = \dot{V}_b^d = 0_6$.

Similiar to the approach in [24], the feedback term is introduced as deviation in position, orientation, and generalized momentum of the robot from the desired trajectory. Let us define the robot pose error $\tilde{X}_r \in \mathbb{R}^6$ and the robot's generalized momentum error $\tilde{h}_r \in \mathbb{R}^6$ relative to the base frame of the platform

$$F_r^{fb} = \mathrm{Ad}_{g_{rb}}^\top K_r \tilde{X}_r + D_r \tilde{h}_r, \tag{14}$$

where $K_r \in \mathbb{R}^{6\times6}$ and $D_r \in \mathbb{R}^{6\times6}$ are symmetric and positive definite gain matrices. As defined in (9), the wrench acting on the robot frame is projected to the base frame.

The desired robot wrench needs to be generated through contact wrenches in the contact points between the robot and the platform as shown in Fig. 2. The relation between the net robot wrench and the contact wrench is given by

$$F_r = \mathrm{Ad}_{g_{cb}}^\top F_c, \tag{15}$$

with $F_c \in \mathbb{R}^6$. The derivation in this section assumes that only one end effector of the robot is in contact with the platform; however, the formulation can be readily extended to other contact configurations.

In order to correct the orientation of the platform after possible disturbances, we define a desired platform wrench resulting from a PD feedback attitude controller. Therefore, the attitude error $\tilde{X}_b \in \mathbb{R}^3$ and angular velocity error $\tilde{\omega}_b \in \mathbb{R}^3$ of the base frame of the platform w.r.t. the inertial frame are introduced

$$F_b^{fb} = K_b \tilde{X}_b + D_b \tilde{\omega}_b, \tag{16}$$

where $K_b \in \mathbb{R}^{3\times3}$ and $D_b \in \mathbb{R}^{3\times3}$ are the symmetric and positive definite gain matrices. Since the translation of the platform is of minor importance for common applications, we only formulate a feedback controller for the orientation. Corresponding to (15), the satellite wrench is mapped to the contact wrench via

$$F_b = -\mathrm{Ad}_{g_{cb}}^\top F_c. \tag{17}$$

The resulting contact wrenches F_c^{opt} can be readily computed by using the pseudo-inverse of the stacked adjoint matrices. However, to incorporate force and torque limits in the SIs, (15) and (17) are solved by using a constraint quadratic optimization problem (QP) formulation:

$$\min_{F_c^{opt}} \sum_{i\in\{r,\,b,\,c\}} \delta_i^T Q_i \delta_i \tag{18}$$

with the residua

$$\delta_r = \mathrm{Ad}_{g_{cb}}^\top F_c^{opt} - F_r^d \tag{19}$$

$$\delta_b = \mathrm{Ad}_{g_{cb}}^\top F_c^{opt} + F_b^d \tag{20}$$

$$\delta_c = F_c^{opt} \tag{21}$$

and with respect to the contact wrench constraints

$$F_c^{min} \le F_c^{opt} \le F_c^{max}. \tag{22}$$

The optimization tries to find a trade-off between the robot trajectory tracking task (19), the platform orientation task (20), and a wrench regulation task (21) based on the weighting matrices Q_r, Q_b and Q_c, which are symmetric and positive definite. The wrench regulation task is added to ensure that the contact forces and torques are minimized as much as possible. The QP formulation is a multi-level task optimization where the contact wrench constraints (22) have the highest priority and are strictly enforced, while the remaining tasks (19)-(21) form a soft hierarchy. Since the platform orientation task is of highest importance, we chose $Q_b >> Q_r, Q_c$. The QP provides a solution for the contact wrenches, which disturb the orientation of the satellite as little as possible, while trying to generate the robot wrench that is required to follow the desired trajectory. Based on the SI specifications, upper and lower limits on the contact wrenches can be enforced through (22).

Following Assumption 2, the optimized contact wrenches resulting from (18) are generated through an additional controller on joint level.

5. NUMERICAL EXPERIMENTS

To demonstrate the effectiveness of the proposed control and optimization scheme, we present several locomotion scenarios and compare the tracking performances. We also show the advantage of our approach in the case of external disturbances.

Implementation

The proposed approach was implemented in a Matlab/Simulink environment. For the dynamic calculation, we used our in-house dynamic library [27]. The Matlab solver *quadprog* is used for solving the QP problem.

Environment

The reference environment is taken from the project MIRROR, including the definition of sizes and masses. The robot mass is taken as $m_r = 200kg$. For representing the robot's inertia, we use a cubic box with edge length $a = 0.3m$. The corresponding inertia tensor of the robot is then

$$I_r = \begin{bmatrix} \frac{1}{6}m_r a^2 & 0 & 0 \\ 0 & \frac{1}{6}m_r a^2 & 0 \\ 0 & 0 & \frac{1}{6}m_r a^2 \end{bmatrix} \tag{23}$$

We assume as desired structure the LUVOIR space telescope [28] (successor of the JWST), with a mirror radius of $r_b = 7.5m$. We also assume a mirror tile with a outer radius $r_t = 1m$ and a height $h_t = 0.3m$ and mass $m_t = 30kg$. 68 mirror tiles are required, leading to a total mass of $m_b = 2040kg$ in the full assembly, with an inertia tensor corresponding to a flat cylinder with a height $h_b = 0.3m$.

$$I_b = \begin{bmatrix} \frac{1}{12}m_b(3r^2 + h^2) & 0 & 0 \\ 0 & \frac{1}{12}m_b(3r^2 + h^2) & 0 \\ 0 & 0 & \frac{1}{2}m_b r^2 \end{bmatrix} \tag{24}$$

Note that for our experiments the weight ratio between the robot and structure is in the medium range. This means that the main mass of the system corresponds to the desired assembly, and the robot mass is smaller but not neglectable. One extreme case would be that the satellite is so light that the robot would move the platform by some degrees while only moving its joints. In the other extreme case, the platform is much heavier than the robot, so that the base disturbance introduced by the robot can be neglected.

For the SI representing the potential supports (and the contact point constraints) we use HOTDOCK [9]. This has a non-destructive load range of 3000N traction and 300 Nm in bending moment. In these experiments we assume to have absolute knowledge about the environment, but for real system a separate grasping controller is needed, which can handle the uncertainties.

Experiment Platform disturbances

In the first experiment, we want to show the tracking performance of the robot while following a predefined trajectory. The effect of the robot motion on the satellite base and the contact wrenches is also considered. The presented framework for contact wrench optimization can be combined with different robot platforms as long as a joint controller can generate the commanded contact wrenches.

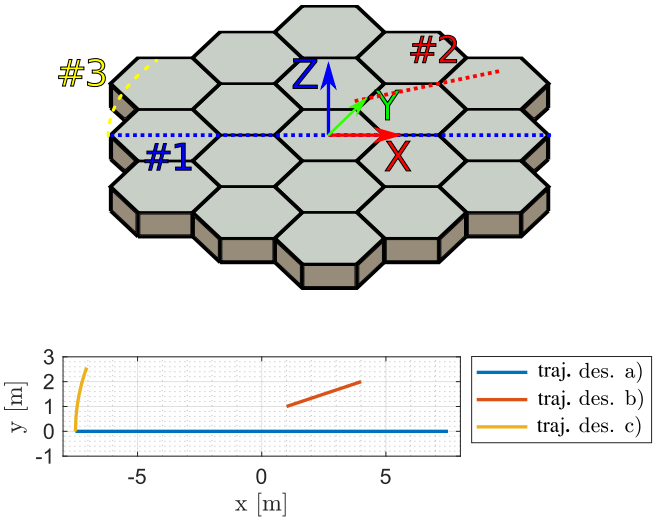

Figure 4: Top: Trajectories considered for locomotion of the MAR on top of the assembly. Bottom: xy-plot showing the three experimental trajectories.

The results describe the translation coordinates as x, y, z and the corresponding rotations as α, β, γ, in Euler angles(roll-pitch-yaw). Since we assume that the z axis is pointing in the direction of communication, a rotation around γ is not optimized. We select three different robot trajectories for walking over the assembly, as shown in Fig. 4.

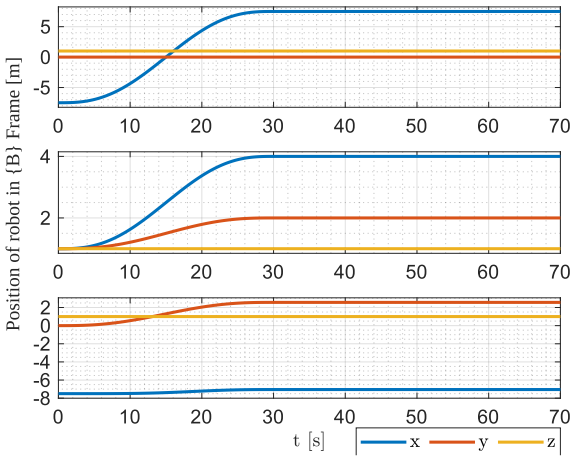

Figure 5: Desired position trajectories of the robot. The robot is moving from start to goal in 30 seconds(see x axis), afterward holding the position, for system stabilization. Top: experiment #1; middle: experiment #2; bottom: experiment #3.

Experiment #1: straight line displacement, crossing the CoM of the assembly
Experiment #2: straight line displacement, on the vicinity of the CoM of the assembly
Experiment #3: circular segment displacement, with center at the CoM of the assembly

These trajectories are basic motions that can be used to build more complex movements. All CoM trajectories are planned and executed at 1-meter height over the satellite surface. We use a PD controller with feed-forward terms to follow the desired trajectory. The robot trajectory over time is shown in Fig. 5, and Fig. 4 illustrates the spatial trajectory on the XY plane (looking from above the telescope). Fig. 4 clearly shows that experiment #1 moves the robot in a straight line over the system CoM ($x_{com} = [0 \quad 0 \quad 0]$). For experiment #2, we see a straight line again, which moves in the x and y directions. Finally, for experiment #3 the circular motion is visible.

Experiment #1—The commanded motion for this experiment is a straight line from $x_{start} = [-7.5 \quad 0 \quad 1]^T$ to $x_{goal} = [7.5 \quad 0 \quad 1]^T$, see Fig. 4. The given trajectories are a 5^{th}-order polynomial with zero acceleration and velocity at the start and end of the motion. The trajectories are executed during 30 seconds, and the rest of the simulation shows the stabilization of the system. The robot moves only in one direction passing over the CoM of the base, so this example could be considered as a two-dimensional problem.

The rotation of the satellite base is shown in Fig. 6. The left side shows the non-optimized behavior, and the right side shows the behavior of the base disturbance in the optimized case. Note that the α and γ rotations are constantly zero. Indeed, there is no lever arm from CoM_b and CoM_r in x and y direction, so no momentum can be produced. On the other hand, we have the motion in the x direction with a

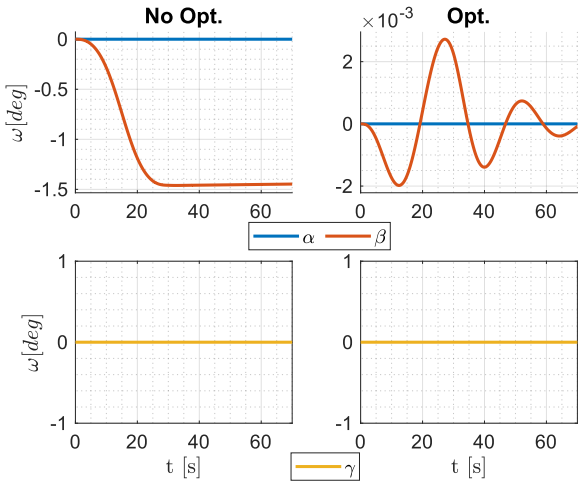

Figure 6: Experiment #1; rotation α, β, γ of the base as a result of the robot motion.

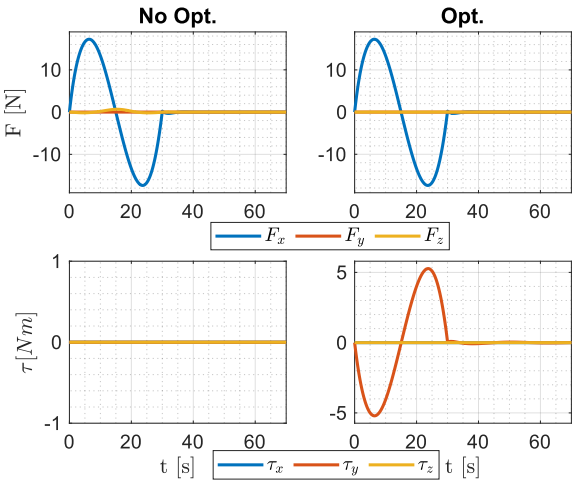

Figure 7: Contact wrench for the non-optimized (left) and optimized case (right) in experiment #1.

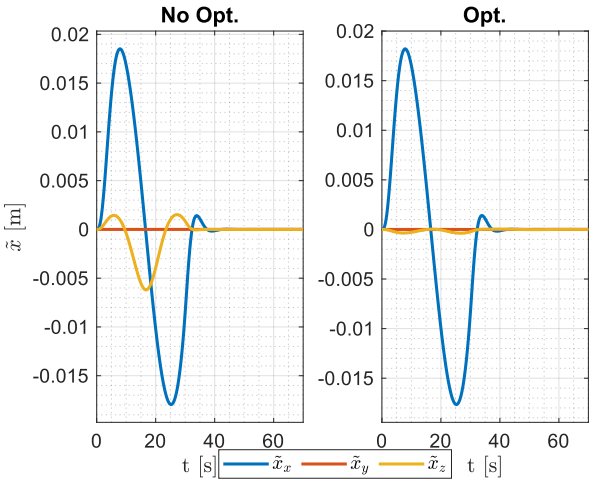

Figure 8: Experiment #1; position tracking error of the robot trajectory.

lever arm in z, which produces momentum in the β axis. This momentum rotates the base from 0 to -5 degrees in the non-optimized part. Note that the base first starts to rotate, accelerating like the robot at the beginning. Then, after around 15 seconds, there is a phase with constant rotation velocity, and in the end, the platform decelerates like the robot is doing as well in order to stop its motion. In the end, around 35 seconds, both the robot and the base have zero velocity. Here the final rotation of the base is around $\beta = -1.5$ degrees For the optimized case on the right side, note that the system swings around 0 degrees with minimal $\beta = -2 \times 10^{-3}$ and maximal $\beta = 2.55 \times 10^{-3}$ degrees amplitude. In the first 30 seconds, the optimizer has to counteract the robot dynamics when following the desired trajectory. After that, the optimizer tries to bring the base to zero degrees, which can be seen in the decreasing oscillation of the platform.

Fig. 7 compares the contact wrenches of the non optimized and optimized experiment. For better visualization, we split them into forces and torques. Note that the force diagrams are similar for the non-optimized and the optimized case. The reason is that the force needed to move the robot forward is the same as the followed trajectory is identical. However, we see that there are differences in the torques. For the non-optimized case, the contact torques do not change as the robot is only commanded to follow a straight line. However, for the optimized case, the robot tries to counteract the base rotation by producing torques at the contact points, as can be seen on the small amplitude oscillations in Fig. 6.

For the tracking controller, Fig. 8 shows the control error in position. Note that the error in x is similar, while the error in z is greatly reduced in the optimized case.

Experiment #2— Now the robot moves in a straight line but with an offset with respect to the CoM, so its motion occurs along the x and y direction. The motion starts at $x_{start} = [1 \quad 1 \quad 1]^T$ and ends in $x_{goal} = [4 \quad 2 \quad 1]^T$, see Fig. 4. Since the trajectory is not directly over the CoM, a momentum is created around all three axes, as illustrated in Fig. 9. The maximum rotation for the non optimized case is about $\alpha_{max} = 0.1$, $\beta_{max} = -0.3$ and $\gamma_{max} = 0.35$ degrees. The γ rotation is not considered for the optimization, so it is the same for both cases. However, note the gain in the optimized case for the rotation axis α and β. The robot is actuated only for 30 seconds, but the underdamped oscillations still drive the system toward equilibrium around 0 degrees.

Forces and torques are shown in Fig. 10. In experiment #1 only F_x and τ_y were used to follow the trajectory and stabilize the platform, but here also F_y and τ_x are required since they produce the force to move the robot in the y axis and to counteract the rotation around α.

The errors in position tracking are shown in Fig. 11. When comparing to experiment #1, in this case there is an error in the y direction since they are now required to follow the desired trajectory. The error magnitude is however smaller than in experiment #1.

Experiment #3—In this experiment the robot follows a circular segment with center on the CoM of the assembly, radius of $r = 7.5$ meters, and 20 degrees in angular amplitude. The robot is then walking 20 degrees on the edge of the telescope, and the motion is executed in 30 seconds. The motion starts

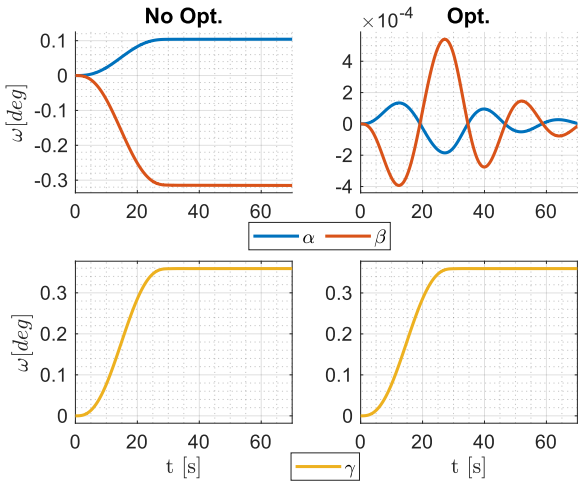

Figure 9: Experiment #2; rotation α, β, γ of the base introduced by the robot.

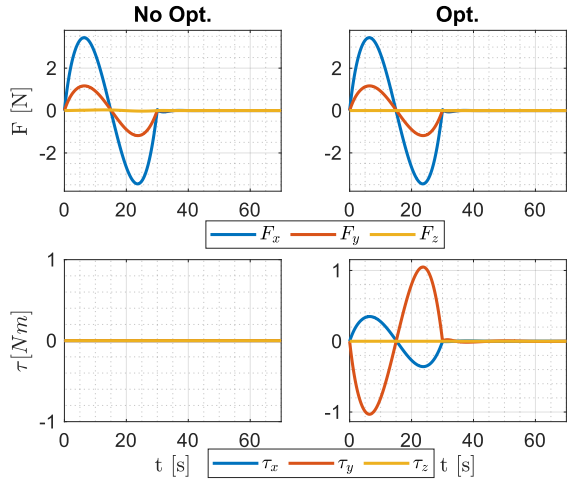

Figure 10: Contact wrench for the non-optimized and optimized case of experiment #2

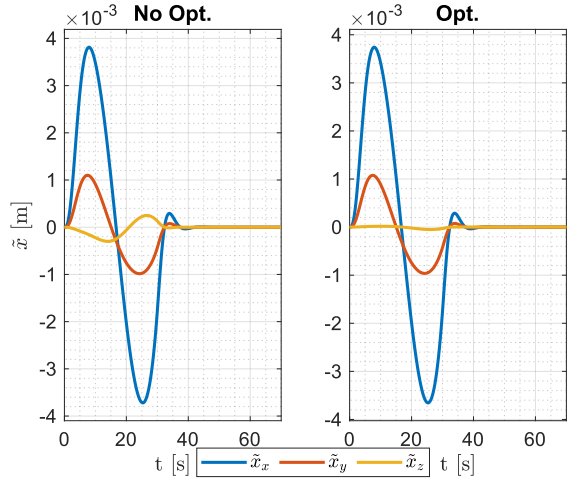

Figure 11: Experiment #2; position tracking error of the robot trajectory.

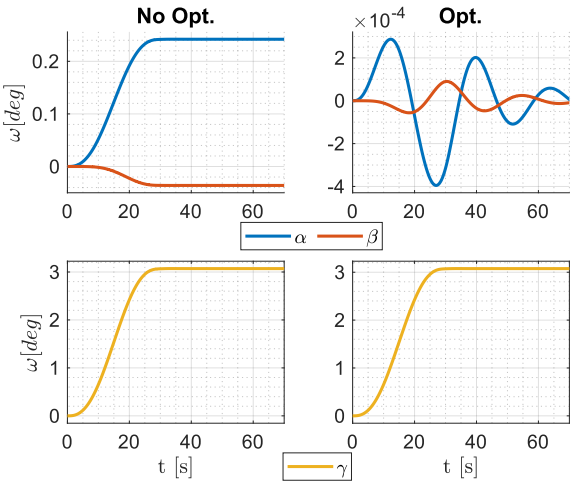

Figure 12: Experiment #3; rotation α, β, γ on the base introduced by the robot.

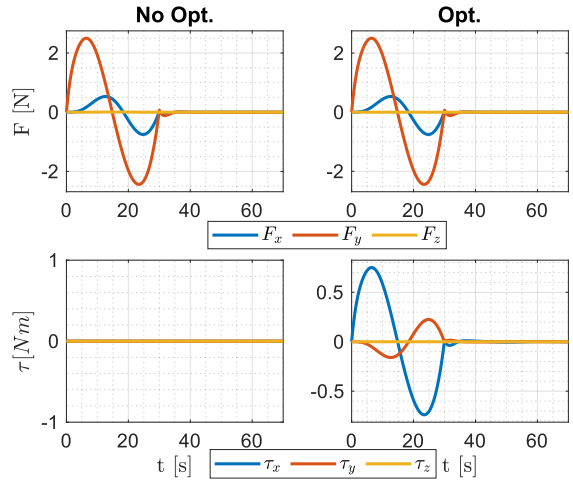

Figure 13: Contact wrench for the non-optimized and optimized case of experiment #3.

at $x_{start} = [0 \quad 0 \quad 1]$, see Fig. 4.

This trajectory has a lever arm around all three axes, so a residual momentum is created around all of them, see Fig. 12. This more demanding motion, compared to experiment #2 , also induces higher rotations on the base in the non-optimized case: $\alpha_{max} = 0.24$, $\beta_{max} = |-0.04|$ and $\gamma_{max} = 0.35$ degrees. For the optimized case, we see again small rotations in all axis, and the optimizer successfully stabilizes the platform.

Fig. 13 shows the contact wrenches. Note that the non optimized case only requires forces to follow the desired trajectory, while the optimized case uses the torques to counteract the rotation of the base.

Fault tolerance

No matter how well the system is designed, there is always a chance of errors during execution. Humans can of course react easily on non-nominal cases, while autonomous systems require certain robustness to potential faults.

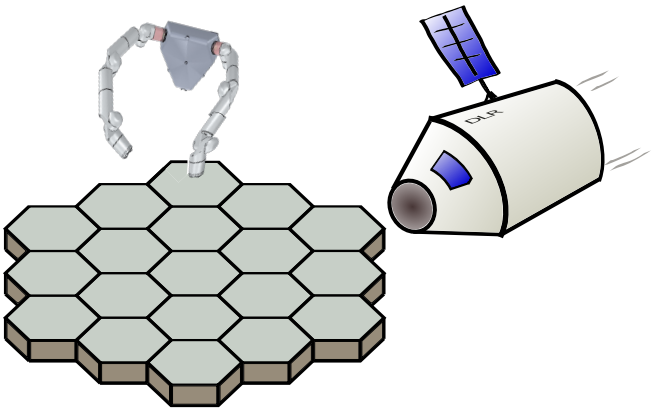

Figure 14: Artistic representation of the robotic assembly of a space telescope, with a servicer satellite docking to provide new parts.

The perturbation scenario analyzed here is as follows. During the assembly process, it might be required that some parts are delivered while the building process takes place. We assume that the robot is actually moving over the platform when a servicer satellite tries to dock to the already built platform (Fig. 14). This docking produces a linear force through the CoM of the base while not changing the mass and inertia of the system. However, this force deflects the robot from its original path and introduces a torque around the combined CoM of the base of the robot. For the analysis, we assume an impact in the $-y$ direction with $1000N$ for 0.1 seconds at the first second of the simulation, and the robot follows the same trajectory from experiment #1.

Fig. 15 shows the rotational disturbances of the base introduced by the motion of the robot and the impact of the servicer satellite. Note that in the non-optimized case after one second α and γ are linearly increasing. This means that the base constantly rotates around these axes. The rotation in β is only produced by the motion of the robot, similar to Fig. 6. Note that in the optimized case α and β are stabilized around zero. This means that our optimizer can handle the external rotational disturbances in the system while fulfilling the required tasks.

The wrenches needed to counteract the impulsive perturbation are represented in Fig. 16. For the forces, the non-optimized and optimized diagrams are quite similar, since they only handle the position error of the robot. A peak at 1 second in F_y direction moves the robot back on the desired trajectory. Since the non-optimized part ignores the rotation of the base, the produced torques are zero. But in the optimized case, the torques required to counteract the robot motion τ_y and the torques to stop the rotation introduced by the servicer τ_x are clearly seen.

Finally, we analyze the convergence of the robot back to the desired trajectory, as shown in Fig. 17. We see for both cases that the impact of the servicer produces an error of -0.03 m in the y direction. The main difference comes in the optimized case for the z component, which is quickly dissipated compared to the non-optimized case. The system is able to reduce the error completely by the end of the trajectory.

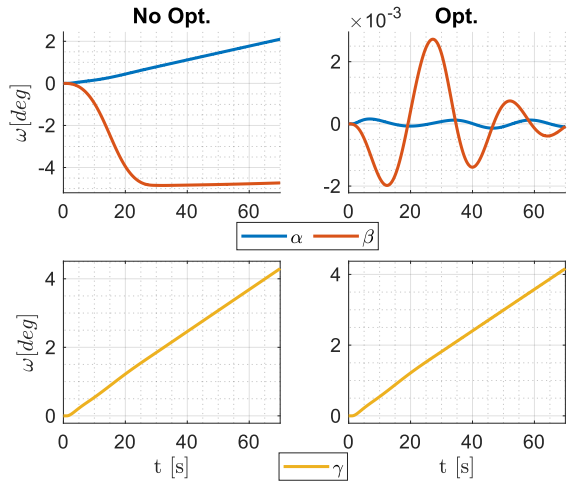

Figure 15: Experiment #1 with external disturbance; rotation α, β, γ of the base introduced by the robot with an initial perturbation coming from a docking satellite.

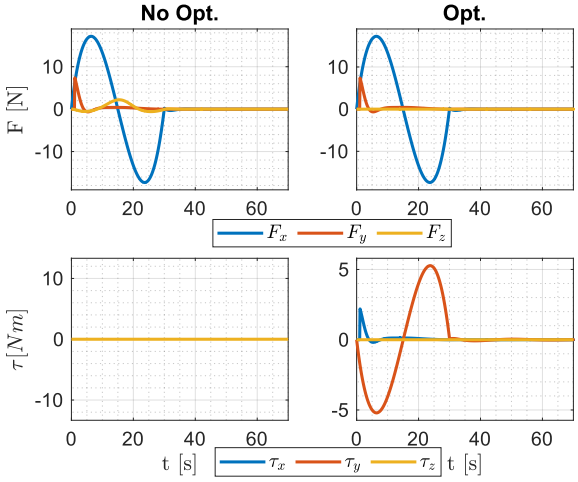

Figure 16: Experiment #1 with external disturbance; contact wrench for the non-optimized and optimized case.

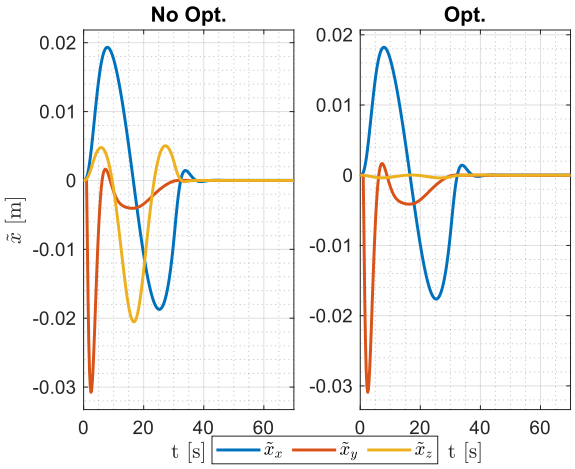

Figure 17: Experiment #1 with external disturbance; position tracking error of the robot trajectory.

6. Conclusions and Future Work

This paper worked on the problem of minimizing perturbations on the satellite base while a robot is performing locomotion tasks on top of it. Given the free-floating space structure with a multi-arm robot, we first derived the consistent equations of motion. Secondly, we proposed simplifications of the system into combined inertia for the space structure and the robot, which enables us to analyze locomotion while considering perturbations to the platform. Additionally, we derived an approximation for a walking contact model with Standard Interconnects. To control the robot motions, we proposed a controller based on Quadratic Programming to optimize the contact wrenches such that a given trajectory of the robot is followed and, at the same time, structural perturbations are reduced.

All of the previous points were validated via multiple numerical experiments where the robot is moving over the floating structure, thus inducing a rotation of the structure by the conservation of momentum. The analyzed scenarios include different trajectories, with different effects on the robot-platform system. In all the cases our optimization approach reduces the induced rotation by introducing suitable contact wrenches at the contact points.

In summary, we have shown a solution for computing the interaction forces between a general robot and any space structure in order to reduce rotational disturbances. In some cases the final control error of these rotational disturbances was nearly zero.

Even though the approach has shown good results, there are still several open points to be tackled in future works. A first task is to investigate robustness of the approach for different failure cases, e.g. a reduced performance of the SI that could limit the applicable forces or torques through the connection points. Also, in our approach we have modeled the robot as a punctual mass to prove the concepts of reduction of satellite disturbances. The consideration of the robot as a multi-body object is ongoing work.

Acknowledgments

The authors want to thank Fabian Beck for his help with the LucaDynamic module used for the numerical experiments in this paper.

References

[1] H. Farivarnejad, A. S. Lafmejani, and S. Berman, "Fully decentralized controller for multi-robot collective transport in space applications," in *Proc. IEEE Aerospace Conf.*, 2021, pp. 1–9.

[2] M. Deremetz, G. Grunwald, F. Cavenago, M. A. Roa Garzon, M. De Stefano, H. Mishra, M. Reiner, S. Govindaraj, A. But, I. Sanz Nieto *et al.*, "Concept of operations and preliminary design of a modular multi-arm robot using standard interconnects for on-orbit large assembly," in *Proc. IAF Int. Astronautical Congress (IAC)*, 2021.

[3] G. Hirzinger, "Rotex — the first space robot technology experiment," in *Experimental Robotics III*, T. Yoshikawa and F. Miyazaki, Eds. Berlin, Heidelberg: Springer Berlin Heidelberg, 1994, pp. 579–598.

[4] M. Oda, K. Kibe, and F. Yamagata, "ETS-VII, space robot in-orbit experiment satellite," in *Proc. IEEE Int. Conf. Robotics and Automation (ICRA)*, vol. 1, 1996, pp. 739–744.

[5] R. P. Hoyt, "Spiderfab: An architecture for self-fabricating space systems," in *AIAA Space Conf.*, 2013, p. 5509.

[6] J. Martínez-Moritz, I. Rodríguez, K. Nottensteiner, J.-P. Lutze, P. Lehner, and M. A. Roa, "Hybrid planning system for in-space robotic assembly of telescopes using segmented mirror tiles," in *Proc. IEEE Aerospace Conf.*, 2021, pp. 1–16.

[7] J. P. Gardner, J. C. Mather, M. Clampin, R. Doyon, M. A. Greenhouse, H. B. Hammel, J. B. Hutchings, P. Jakobsen, S. J. Lilly, K. S. Long *et al.*, "The James Webb Space telescope," *Space Science Reviews*, vol. 123, no. 4, pp. 485–606, 2006.

[8] I. Rodríguez, A. S. Bauer, K. Nottensteiner, D. Leidner, G. Grunwald, and M. A. Roa, "Autonomous robot planning system for in-space assembly of reconfigurable structures," in *Proc. IEEE Aerospace Conf.*, 2021, pp. 1–17.

[9] P. Letier, T. Siedel, M. Deremetz, E. Pavlovskis, B. Lietaer, K. Nottensteiner, M. A. Roa Garzon, J. Sánchez Garcia, J. L. Corella, and J. Gancet, "Hotdock: Design and validation of a new generation of standard robotic interface for on-orbit servicing," in *Proc. IAF Int. Astronautical Congress (IAC)*, 2020.

[10] J. Lenda, "Manned Maneuvering Unit: User's guide," Tech. Rep., 1978.

[11] B. Griffin, "Benefits of a single-person spacecraft for weightless operations," in *Int. Conf. on Environmental Systems*, 2012, p. 3630.

[12] G. Gibbs and S. Sachdev, "Canada and the International Space Station program: overview and status," *Acta Astronautica*, vol. 51, no. 1-9, pp. 591–600, 2002.

[13] R. Boumans and C. Heemskerk, "The European Robotic Arm for the International Space Station," *Robotics and Autonomous systems*, vol. 23, no. 1-2, pp. 17–27, 1998.

[14] P. Letier, X. T. Yan, M. Deremetz, A. Bianco, G. Grunwald, M. Roa, R. Krenn, M. M. Arancón, P. Dissaux, J. S. G. Casarrubios *et al.*, "MOSAR: Modular spacecraft assembly and reconfiguration demonstrator," in *Proc. Symp. on Advanced Space Technologies in Robotics and Automation (ASTRA)*, 2019.

[15] H. Mishra, M. De Stefano, and C. Ott, "Dynamics and control of a reconfigurable multi-arm robot for in-orbit assembly," *IFAC-PapersOnLine*, vol. 55, no. 20, pp. 235–240, 2022.

[16] I. Rodríguez, J.-P. Lutze, H. Mishra, P. Lehner, and M. A. Roa, "Hybrid planning to minimize platform disturbances during in-orbit assembly tasks," in *Proc. IEEE Aerospace Conf.*, 2022, pp. 1–11.

[17] M. Kalakrishnan, S. Chitta, E. Theodorou, P. Pastor, and S. Schaal, "STOMP: Stochastic trajectory optimization for motion planning," in *Proc. IEEE Int. Conf. Robotics and Automation (ICRA)*, 2011, pp. 4569–4574.

[18] D. Mayne, J. Rawlings, C. Rao, and P. Scokaert, "Constrained model predictive control: Stability and optimality," *Automatica*, vol. 36, no. 6, pp. 789–814, 2000.

[19] R. Schuller, G. Mesesan, J. Englsberger, J. Lee, and C. Ott, "Online centroidal angular momentum reference generation and motion optimization for humanoid push

recovery," *IEEE Robot. Autom. Lett.*, vol. 6, no. 3, pp. 5689–5696, 2021.

[20] B. Henze, M. A. Roa, and C. Ott, "Passivity-based whole-body balancing for torque-controlled humanoid robots in multi-contact scenarios," *Int. J. Robotics Research*, vol. 35, no. 12, pp. 1522–1543, 2016.

[21] R. Schuller, G. Mesesan, J. Englsberger, J. Lee, and C. Ott, "Online learning of centroidal angular momentum towards enhancing DCM-based locomotion," in *Proc. IEEE Int. Conf. Robotics and Automation (ICRA)*, 2022, pp. 10 442–10 448.

[22] P. From, I. Schjlberg, J. Gravdahl, K. Pettersen, and T. Fossen, "On the boundedness and skew-symmetric properties of the inertia and coriolis matrices for vehicle-manipulator systems," *Proc. IFAC Symp. on Intelligent Autonomous Vehicles*, vol. 43, no. 16, pp. 193–198, 2010.

[23] R. Featherstone, *Rigid Body Dynamics Algorithms*. Berlin, Heidelberg: Springer-Verlag, 2007.

[24] G. Garofalo, B. Henze, J. Englsberger, and C. Ott, "On the inertially decoupled structure of the floating base robot dynamics," *IFAC-PapersOnLine*, vol. 48, no. 1, pp. 322–327, 2015.

[25] C. Ott, M. A. Roa, and G. Hirzinger, "Posture and balance control for biped robots based on contact force optimization," in *Proc. IEEE-RAS Int. Conf. on Humanoid Robots*, 2011, pp. 26–33.

[26] B. Paden and R. Panja, "Globally asymptotically stable PD+ controller for robot manipulators," *Int. J. Control*, vol. 47, no. 6, pp. 1697–1712, 1988.

[27] G. Garofalo, C. Ott, and A. Albu-Schffer, "On the closed form computation of the dynamic matrices and their differentiations," in *Proc. IEEE/RSJ Int. Conf. on Intelligent Robots and Systems (IROS)*, 2013, pp. 2364–2359.

[28] M. R. Bolcar, S. Aloezos, V. T. Bly, C. Collins, J. Crooke, C. D. Dressing, L. Fantano, L. D. Feinberg, K. France, G. Gochar *et al.*, "The large uv/optical/infrared surveyor (LUVOIR): decadal mission concept design update," in *UV/Optical/IR Space Telescopes and Instruments: Innovative Technologies and Concepts*, vol. 10398. SPIE, 2017, pp. 79–102.

Jean-Pascal Lutze *received his B.Eng degree in Robotic and Automation from Heilbronn University of Applied Sciences. Since 2017, he is part of the Institute of Robotics and Mechatronics at the German Aerospace Center (DLR). He obtained his Master degree in Robotics, Cognition, Intelligence at the Technical Univ. of Munich (TUM) in 2022. His main research focus is space robotics.*

Robert Schuller *received his M.Sc. in Mechanical Engineering from the Technical Univ. of Munich (TUM), Germany in 2020. He joined the Institute of Robotics and Mechatronics of the German Aerospace Center (DLR) as research scientist in 2020. His research interests include humanoid robots, legged locomotion and whole-body control.*

Hrishik Mishra *is a research associate at the German Aerospace Center (DLR), focused on orbital robotic systems. He received his M.Sc. in Satellite Application Engineering from the Technical Univ. of Munich (TUM) in 2017. In 2010 he received his B.Tech. in Electrical and Electronics Engineering from the Biju Patniak Univ. of Technology (BPUT), India. At DLR, his research is directed towards whole-body control, shared control, and hardware-in-the-loop simulation of orbital robots.*

Ismael Rodríguez *received his degree of Ingeniero en Electrónica from Universidad ORT Uruguay in 2015. Since 2016 he is pursuing a Ph.D. in Robotics at the German Aerospace Center (DLR) in Weßling. His research is focused on the development of an assembly planner that is aligned with the requirements of the mass customization phenomenon.*

Máximo A. Roa-Garzón *received his doctoral degree in 2009 from Universitat Politecnica de Catalunya (UPC), and the Project Management Professional (PMP) Certification in 2016. He worked for Hewlett Packard R&D before joini ng the Institute of Robotics and Mechatronics of the German Aerospace Center (DLR) in 2010 as Senior Research Scientist, leading the group on Robotic Planning and Manipulation.*